Strength optimization of ultralight corrugated-channel-core sandwich panels

ZHAO ZhenYu[1,2], LI Lang[1,2], WANG Xin[1,2], ZHANG QianCheng[1,2*], HAN Bin[3,4] & LU TianJian[2,3,1*]

[1] State Key Laboratory for Strength and Vibration of Mechanical Structures, Xi'an Jiaotong University, Xi'an 710049, China;

[2] State Key Laboratory of Mechanics and Control of Mechanical Structures, Nanjing University of Aeronautics and Astronautics, Nanjing 210016, China;

[3] Nanjing Center for Multifunctional Lightweight Materials and Structures (MLMS), Nanjing University of Aeronautics and Astronautics, Nanjing 210016, China;

[4] School of Mechanical Engineering, Xi'an Jiaotong University, Xi'an 710049, China

Novel ultralight sandwich panels, which are comprised of corrugated channel cores and are faced with two identical solid sheets, subjected to generalized bending are optimally designed for minimum mass. A combined analytical and numerical (finite element) investigation is carried out. Relevant failure mechanisms such as face yielding, face buckling, core yielding and core buckling are identified, the load for each failure mode derived, and the corresponding failure mechanism maps constructed. The analytically predicted failure loads and failure modes are validated against direct finite element simulations, with good agreement achieved. The optimized corrugated channel core is compared with competing topologies for sandwich construction including corrugations, honeycombs and lattice trusses, and the superiority of the proposed structure is demonstrated. Corrugated-channel-core sandwich panels hold great potential for multifunctional applications, i.e., simultaneous load bearing and active cooling.

sandwich panel, corrugated channel, generalized bending, optimization

1 Introduction

With growing demand for multifunctional structures (e.g., thermal protection systems for hypersonic vehicles, liquid rocket engine thrust chambers, and ventilated brake discs for high-speed trains and heavy-duty trucks), all-metallic lightweight sandwich panels having fluid-through core topologies receive increasing attention [1,2]. At present, the prevalent all-metallic sandwich cores with multifunctional attributes (e.g., lightweight combined with simultaneous load bearing and active cooling) include 2D (two-dimensional) prismatic cores such as honeycombs (in which the cooling fluid passes along the axial direction of core webs) [3] and folded panels (e.g., corrugations and corrugation channels [4]) as well as 3D (three-dimensional) lattice cores such as pyramidal trusses [5,6] and X-lattices [7,8].

For typical example, 2D prismatic core sandwich panels have been widely studied for structural performance evaluation, active cooling design and bi-functional optimization [9]. When subjected to either transverse or longitudinal bending, structural optimization (minimum weight design) of corrugated core sandwich panels was analytically performed by considering four failure mechanisms: face yielding (FY), face buckling (FB), core member yielding (CY),

and core member buckling (CB) [10]. Subsequently, the three-point bending response of steel corrugated core sandwich panels was characterized, both experimentally and numerically [11]. Further, corrugated core sandwich panels under either out-of-plane compression [12] or in-plane compression [13] were optimally designed for minimum weight.

For active cooling, Lu [14] firstly evaluated the heat transfer efficiency of metal honeycombs by developing a modified fin model. Subsequently, built upon Lu's modified fin model, Gu et al. [15] extended the approach and proposed a two-stage method to optimize, simultaneously, the heat transfer and structural performance of metal honeycombs. Similarly, for corrugated core sandwich panels, optimal geometries that maximize active cooling for a wide range of pumping power were identified and then applied to carry out design optimization for combined heat dissipation and structural loading [16]. Considering the increasing compact demand of heat sinks, Wen et al. [17] adopted the method of intersection-of-asymptotes to perform optimal design of 2D prismatic sandwich panels cooled by forced convection, with the effects of developing flow accounted for. In addition to sandwich panels, for combustion chamber applications, pressurized cylindrical shells with prismatic-cored sandwich walls were also optimized for minimum weight [18] and bi-functional attribute [19]. It was demonstrated that square-celled core sandwich cylinders outperform those having triangular cells in terms of bi-functional design (e.g., simultaneous loading bearing and active cooling). Under out-of-plane compression and shear loading, a corrugated core exhibits weaker buckling modes and so lower strength-to-weight ratio than pyramidal and honeycomb cores [12]. Targeting 2D prismatic cores, Tan and Soh [20] proposed a multi-objective optimization approach to minimize weight and maximize heat transfer at the same time using genetic algorithms.

The weight rankings of strength-optimized sandwich panels with a range of core topologies subject to generalized bending were presented by Rathbun et al. [21]. For constituent materials having a yield strain of $\varepsilon_{ys} = 0.001$, the weight of transverse or longitudinal corrugated core was found to be heavier than square honeycomb core, since the failure modes of buckling (including FB and CB) dominate in the low load domain. Most recently, to address the structural deficiency of corrugated cores, Zhao et al. [4] proposed a novel sandwich core, namely, the corrugated channels as shown in Figure 1. From the heat transfer point of view, the corrugated channels are superior to the popular parallel-plate channels under the design criteria of equal mass flow rate, equal pressure drop, and equal pumping power [22]. From a structural perspective, compared with competing core topologies such as square honeycombs,

pyramidal trusses and folded plates, the corrugated channel core exhibits excellent resistance to buckling and superior out-of-plane compressive performance, particularly so in the low density regime.

To further characterize the structural performance of corrugated-channel-core sandwich panels (3CSPs) proposed in our previous research [4], the current study aims to optimally design 3CSPs for minimum mass subject to generalized bending (Figure 1(a)). A combined analytical and numerical approach is adopted. In Sect. 2, strength failure criteria for 3CSPs subject to generalized bending are analytically derived. Built upon these failure criteria, Sect. 3 presents the design optimization and the failure mechanism maps. In Sect. 4, the accuracy of analytic predictions is validated against direct 3D finite element (FE) simulation results. Finally, in Sect. 5, the optimized 3CSP is compared with competing topologies in terms of structural efficiency.

2 Failure mechanisms of corrugated-channel -core sandwich panel

2.1 Stresses in the faces and corrugated channel core

Figure 1 depicts the proposed 3CSP with height H, face thickness t_f, core web thickness t_c, core height h, inclination angle θ and hypotenuse length s of corrugation web. The equivalent neutral surfaces of the corrugation webs are par-
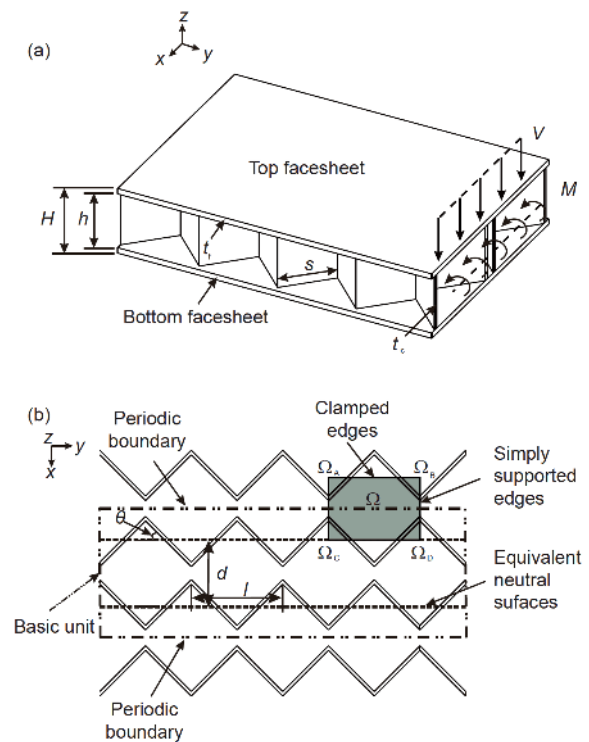
Figure 1 (Color online) (a) Schematic of sandwich panel with triangular corrugated channel core subjected to generalized bending; (b) top view of corrugated channel core.

allel to each other with spacing d. The faces and the core webs are made from the same material. As shown in Figure 1, generalized bending along the longitudinal direction is considered, represented by length scale $\chi \equiv M/V$, M and V being the maximum moment and maximum transverse shear force per unit width, respectively. In addition to carry the mechanical loads, the 3CSP can also dissipate heat from one or both of the heated faces when coolant is forced through the core.

For strength-based sandwich design, it is reasonable to assume that the bending moment and transverse shear are carried almost entirely by the faces and core members, respectively. In addition, perfect bonding is assumed between the faces and core webs so that delamination failure does not occur. The maximum stress in the face is thence

$$\sigma_f = \frac{M}{t_f(h+t_f)} = \frac{V\chi}{t_f(h+t_f)}, \tag{1}$$

while that in the core is [23,24]

$$\tau_c = \frac{Vd}{t_c h}. \tag{2}$$

2.2   Failure criteria

Under generalized bending, four failure modes are considered: face yielding (FY), core yielding (CY), face buckling (FB) and core buckling (CB). Correspondingly, the failure initiation criteria are summarized as below.

Face yielding occurs when

$$\sigma_{fy} = \sigma_{ys}, \tag{3}$$

where σ_{ys} is the uniaxial tensile yield strength of the parent metal.

At the onset of core yielding, the critical stress is

$$\tau_{cy} = \tau_{ys}, \tag{4}$$

where τ_{ys} is the shear yield strength of the parent metal, which is assumed to depend upon the tensile yield strength as $\tau_{ys} = \sigma_{ys}/\sqrt{3}$.

With reference to Figure 1(b), to model the constraint of core web on face sheet, a rectangular pattern Ω with dimensions d by l may be used to characterize approximately the buckling mode of the face sheet. As a result, the critical stress at the onset of face buckling is obtained as

$$\sigma_{fb} = \frac{k_{fb}\pi^2 E_s}{12(1-v_s^2)}\left(\frac{t_f}{d}\right)^2, \tag{5}$$

where E_s and v_s are the Young's modulus and Poisson ratio of the parent material, respectively, and k_{fb} is the face compression buckling coefficient, which depends upon the aspect ratio d/l and boundary conditions. Following Wicks and

Hutchinson [25], the edges parallel to the equivalent neutral surfaces of the core webs (i.e., $\Omega_A\Omega_B$ and $\Omega_C\Omega_D$) are treated as clamped, while the remaining edges (i.e., $\Omega_A\Omega_C$ and $\Omega_B\Omega_D$) are taken as simply supported. Consequently, the face buckling coefficient k_{fb} is approximately equal to 6.97 [26].

Because the core webs can be divided into multiple rectangular thin plates, core buckling is assumed to be associated with the failure mode of a rectangular plate subject to uniform shear stressing. The critical stress at the onset of core buckling is thence:

$$\tau_{cb} = \frac{k_{cb}\pi^2 E_s}{12(1-v_s^2)}\left(\frac{t_c}{h}\right)^2, \tag{6}$$

where the shear buckling coefficient k_{cb} is a function of h/s. It has been suggested that the constraint between the face sheet and the core is closer to the clamped boundary, and so is the constraint between the core members. For a rectangular thin plate with aspect ratio $h/s = 1$, k_{cb} has a value of 14.71 [27].

With the aspect ratio fixed at $h/s = 1$, the four failure criteria can be re-written in non-dimensional form as

$$\frac{V^2}{E_s M} = \frac{\sigma_{ys}}{E_s}\bar{t}_f(\bar{h}+\bar{t}_f), \text{ face yielding,}$$

$$\frac{V^2}{E_s M} = \frac{\sigma_{ys}}{\sqrt{3}E_s}\bar{t}_c\frac{1}{n}, \text{ core yielding,}$$

$$\frac{V^2}{E_s M} = \frac{k_{fb}\pi^2}{12n^2(1-v_s^2)}(\bar{h}+\bar{t}_f)\frac{\bar{t}_f^3}{\bar{h}^2}, \text{ face buckling,} \tag{7}$$

$$\frac{V^2}{E_s M} = \frac{k_{cb}\pi^2}{12n(1-v_s^2)}\frac{\bar{t}_c^3}{\bar{h}^2}, \text{ core buckling.}$$

Relevant non-dimensional geometric parameters are: $\bar{t}_f = t_f/\chi$, $\bar{h} = h/\chi$, $\bar{t}_c = t_c/\chi$, $n = d/h$. The influence of material properties and external loads are embodied by the two non-dimensional quantities: σ_{ys}/E_s and $V^2/E_s M$.

3   Design optimization

3.1   Objective functions and constraints

To determine the geometric parameters which minimize the weight of 3CSP as a function of load index $V^2/E_s M$, optimal design is carried out. The weight per unit area of the sandwich beam is given by $W = 2t_f\rho_s + \frac{t_c h}{d\cos\theta}\rho_s$, where ρ_s denotes the density of the parent material. Written in non-dimensional form, it becomes

$$\psi = \frac{W}{\rho_s\chi} = 2\bar{t}_f + \frac{\bar{t}_c}{n\cos\theta}. \tag{8}$$

To withstand the generalized bending without failure, the stresses in all parts of the sandwich should be less than the

critical values for each failure mode.

Strength-based minimum weight design is performed using a sequential quadratic programming (SQP) algorithm coded in MATLAB, subjected to the following constraints:

$$\frac{V^2}{E_sM}\frac{E_s}{\sigma_{ys}}\frac{1}{\bar{t}_f(\bar{h}+\bar{t}_f)} \leq 1, \quad \text{face yielding,}$$

$$\frac{V^2}{E_sM}\frac{\sqrt{3}E_s}{\sigma_{ys}}\frac{n}{\bar{t}_c} \leq 1, \quad \text{core yielding,}$$

$$\frac{V^2}{E_sM}\frac{12n^2(1-v_s^2)}{k_{fb}\pi^2}\frac{1}{\bar{h}+\bar{t}_f}\frac{\bar{h}^2}{\bar{t}_f^3} \leq 1, \quad \text{face buckling,} \tag{9}$$

$$\frac{V^2}{E_sM}\frac{12n(1-v_s^2)}{k_{cb}\pi^2}\frac{\bar{h}^2}{\bar{t}_c^3} \leq 1, \quad \text{core buckling.}$$

It should be pointed out that, for this type of optimization problems with multiple constraints, it is usually difficult to guarantee the convergence rate of optimization iterations. Consequently, the iteration history of the design objective is systematically examined for different levels of non-dimensional weight. It is demonstrated that, for the optimization problem considered in the present study, the convergence rate of iterations is in general fast.

3.2   Influence of $n=d/h$

To ensure suitably thin sandwich panel designs, the optimization is carried out by imposing an upper limit on core web height, $\bar{h}=0.2$ [10]. Ti-6Al-4V alloy (yield strain $\varepsilon_{ys}=0.007$ and Poisson ratio $v_s=0.34$) is selected as the parent material and the inclination angle of corrugation is fixed at $\theta=45°$. The effect of $n=d/h$ is quantified first, which represents essentially the spacing between two adjacent core webs (Figure 1). Figure 2 presents the optimization results for $n=1, 2, 3$ and 4. As shown in Figure 2(a), the structural efficiency of 3CSP decreases significantly with increasing n, especially so in the relatively low load domain. The effect of n gradually diminishes as the applied load is increased. Analogously, as n is increased, both the face thickness and core web thickness increase monotonically with load, as shown in Figure 2(b) and (c). That is, the optimal face thickness and core web thickness both increase as n is increased. However, correspondingly, the optimal height of core web decreases as shown in Figure 2(d). In the relatively high load domain, the height limit (i.e., $\bar{h}=0.2$) is attained sequentially from $n=1$ to 4.

The results of Figure 2 reveal that, when n is increased, the
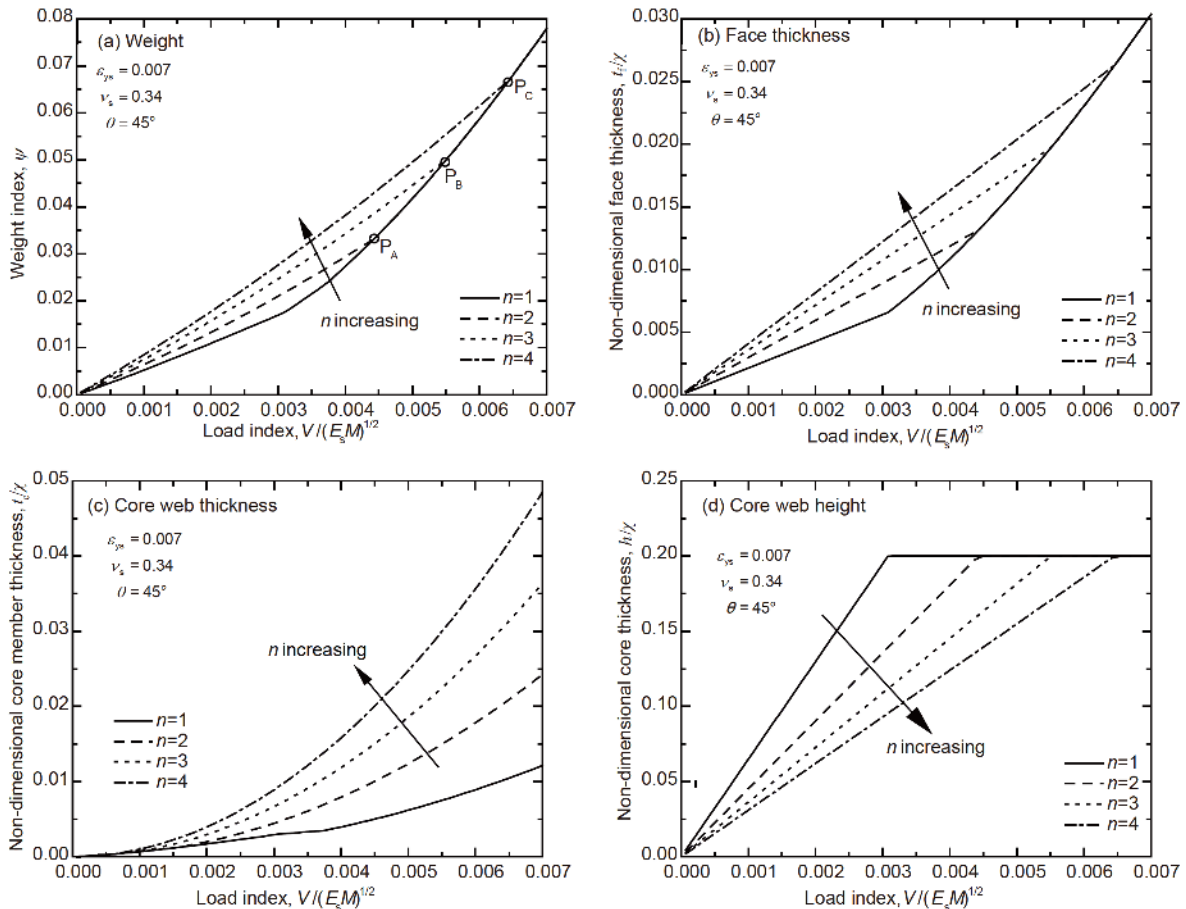
Figure 2   Effect of $n=d/h$ on the optimization of 3CSP subjected to longitudinal bending. Results are presented for titanium alloy ($\varepsilon_{ys}=0.007$, $v_s=0.34$) and fixed inclination angle $\theta=45°$. (a) Minimum weight; (b) optimal face thickness; (c) optimal core web thickness; (d) optimal core web height.

minimum weight of the sandwich no longer varies if the applied load reaches a certain value. For example, the two sandwiches of $n = 1$ and $n = 2$ have the same minimum weight, represented by Point P_A in Figure 2(a). Similarly, Points P_B and P_C are the superiority turning points (STP) for the two structures having $n = 3$ and $n = 4$, respectively. In general, the active failure modes of a sandwich panel under bending are different in different load domains [21,28]. To reveal this phenomena in 3CSP, the influence of each failure criterion on the optimal design of 3CSP is presented in Figure 3 for selected values of $n = d / h$, in which the optimal curve in multicriteria optimization is obtained at the confluence of active failure mechanisms. Note that the turning point of the optimal curve is closely related to active failure modes. The weight range for all kinds of 3CSPs can be divided into three domains. As shown in Figure 3(a), the active failure modes for $n = 1$ are FY, FB and CB in the first domain (domain I). When the load index $V / (E_s M)^{1/2} \approx 0.003$, the core web height limit $\bar{h} = 0.2$ is attained as shown in Figure 2 (d). As a result, this geometrical parameter entails a restriction to FB, resulting in only FY and CB in the second domain (domain II). The transition to the third domain (domain III) starts when the core failure mode changes from CB to CY

and then to a combination of FY and CY. The active failure modes in the second domain of 3CSPs with $n = 2, 3, 4$ are different from 3CSPs with $n = 1$, as shown in Figure 3(b)–(d), where FY, FB and CY are active. Moreover, as $n = d / h$ is increased from 2 to 4, the second domain gradually dominates. After a comprehensive analysis of the results in Figures 2 and 3, the occurrence of SPTs is found under two conditions: (1) producing same active failure modes (FY and CY in the third domain), and (2) attaining the limit of core height.

3.3 Influence of inclination angle θ and yield strain

Next consider the effect of inclination angle θ on minimum weight design. In Figure 4, selected results for $\theta =20°$, $30°$, $40°$, $50°$ and $60°$ are presented. The structural efficiency of 3CSP is slightly influenced by the inclination angle: as θ is increased, the structurally efficiency decreases, but the sensitivity of minimum weight to θ increases.

With $\theta =45°$, the influence of yield strain of the parent metal on 3CSP design is shown in Figure 5. The corresponding result of a solid monolithic plate with yield strain $\varepsilon_{ys} = 0.007$ is also presented. The weight index ψ is related
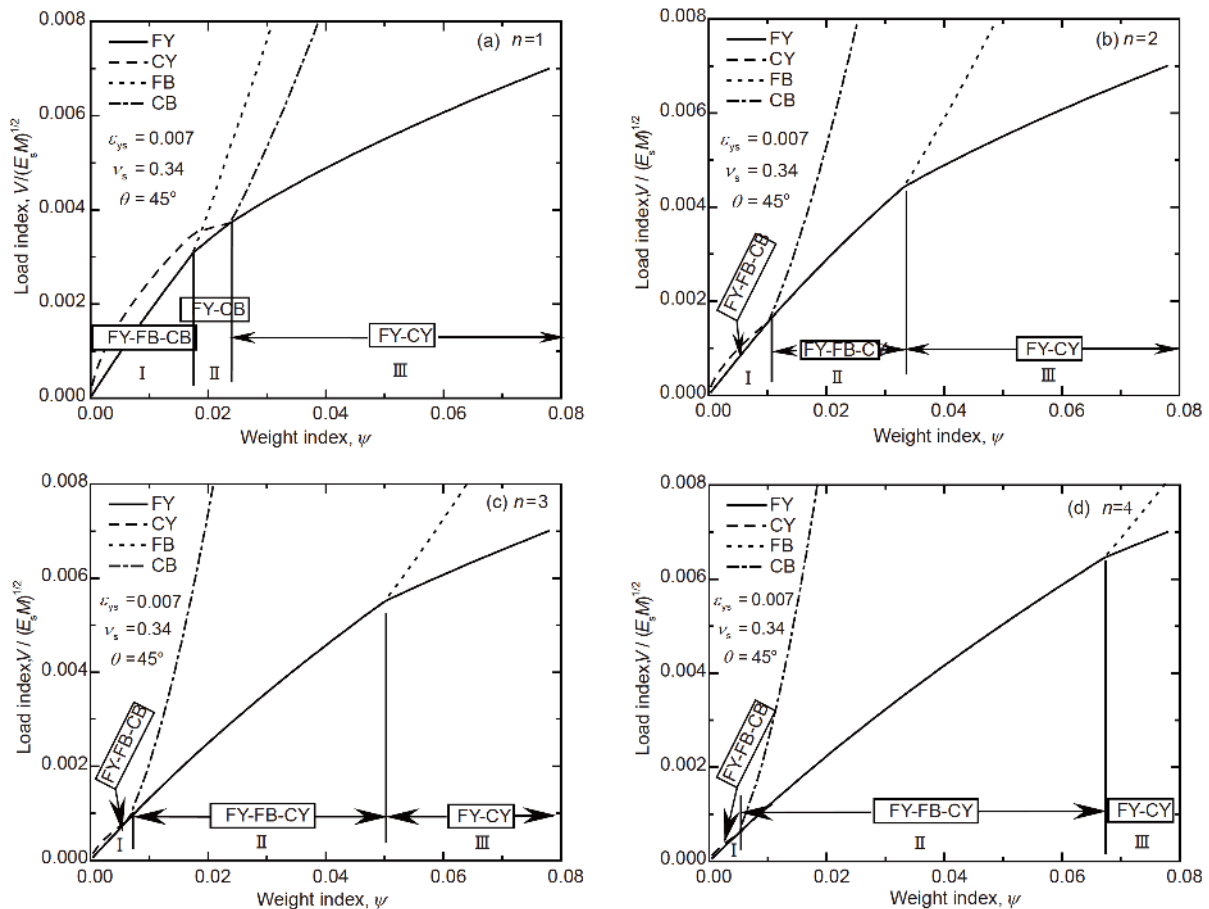
Figure 3 Influence of failure criteria on optimal design of 3CSP for: (a) $n = 1$; (b) $n = 2$; (c) $n = 3$; (d) $n = 4$.
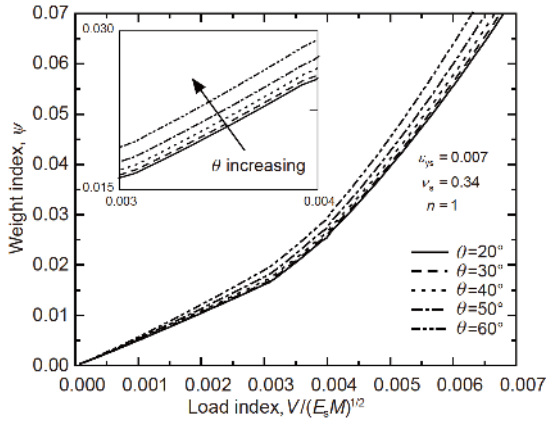
Figure 4   Effect of inclination angle θ on minimum weight of 3CSP subjected to generalized bending.
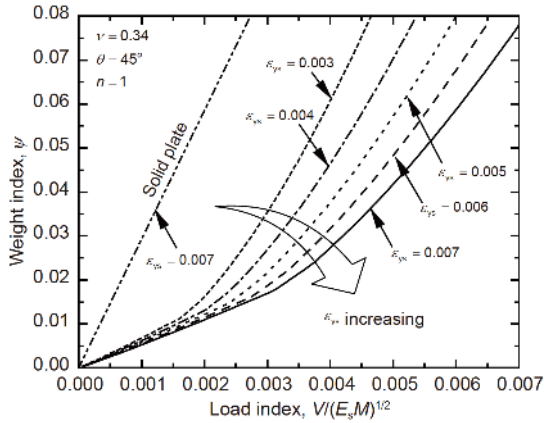
Figure 5   Effect of yield strain on optimal design on 3CSP subjected to generalized bending.

to the load index V^2/E_sM by [29]

$$\psi = \sqrt{\frac{6}{\varepsilon_{ys}}} \frac{V}{(E_sM)^{1/2}}. \tag{10}$$

Figure 5 reveals that the effect of yield strain has remarkable effect on minimum weight design. 3CSPs having a yield strain of $\varepsilon_{ys} = 0.007$ perform best, and the structural efficiency decreases with decreasing ε_{ys}.

3.4   Failure mechanism map

To visualize the optimization results and comprehend the failure modes, failure mechanism maps of Ti-6Al-4V 3CSPs are drawn for selected values of weight index, with $n = 1$, $\varepsilon_{ys} = 0.007$ and $\theta = 45°$. To design the 3CSPs using fixed non-dimensional weight, these maps are defined by $\bar{t}_f$ and $\bar{h}$ coordinates and the boundaries are calculated by progressively equating pairs of constraint functions, as shown in Figure 6. The three maps differ only in non-dimensional weight: $\psi = 0.01$ for Figure 6(a), $\psi = 0.02$ for Figure 6(b) and
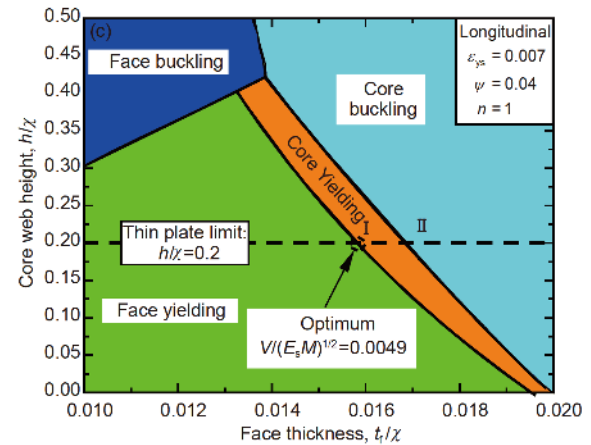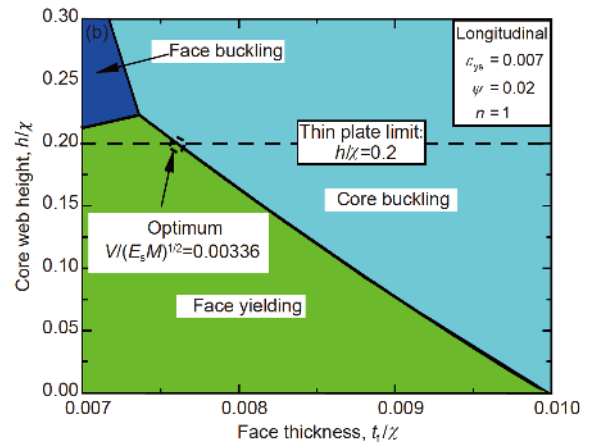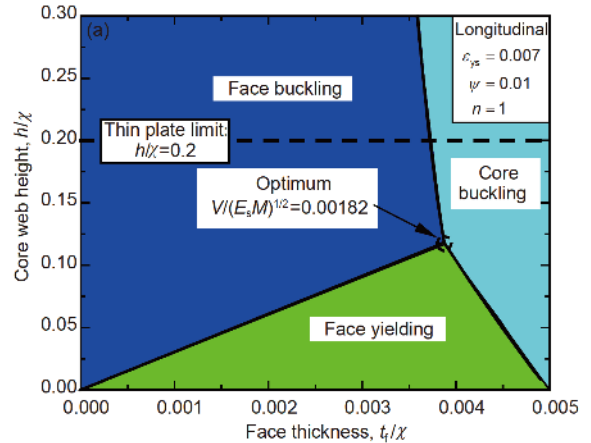
Figure 6   (Color online) Failure mechanism map for 3CSPs ($n = 1$, $\theta = 45°$) made from Ti-6Al-4V alloy ($\varepsilon_{ys} = 0.007$, $v_s = 0.34$). (a) Weight index $\psi = 0.01$; (b) weight index $\psi = 0.02$; (c) weight index $\psi = 0.04$.

$\psi = 0.04$ for Figure 6(c). They correspond to the typical non-dimensional weights of different domains in Figure 3(a). The thin plate limit $\bar{h} = h/\chi = 0.2$ is added to the maps by dashed line.

For each failure mechanism, the regions of its dominance are plotted on the maps. For $\psi = 0.01$ (Figure 6(a)), the optimal sizes are located at the confluence of face yielding, face

buckling and core buckling, and the height limit of core web is not reached. As the weight index is increased to $\psi = 0.02$ (Figure 6(b)). The active failure modes include face buckling, face yielding and core buckling within the range of $\bar{h} \leq 0.3$. However, when the height limit of core web is taken into account, face buckling is restricted. The optimum load is located at a juncture of height limit and the boundary between face yielding and core buckling. A similar situation is observed in Figure 6(c) wherein face buckling is restricted because of the height limit. Point I is located at the confluence of face yielding, core yielding and height limit, and Point II at the confluence of core buckling, core yielding and height limit. For $\psi = 0.04$, the final optimal design parameter is a trade-off between Point I and Point II.

3.5 Indentation

The preceding analysis for generalized bending does not consider indentation failure, which may occur when the face sheet is subjected to local loading such as 3- or 4-point bending. To address this deficiency, optimal design of 3CSPs subjected to combined generalized bending and indentation is performed, as detailed in Appendix. In Figure 7, the optimal design results of 3CSPs ($n = 1$, $\theta = 45°$) made from Ti-6Al-4V alloy subjected to generalized bending are compared with the results obtained for simultaneous generalized bending and indentation. For the latter, the normalized loading platen width is varied as $\bar{a} = 0.01$, 0.05 and 0.1. It is seen from Figure 7 that indentation affects significantly the optimal results. When $\bar{a} = 0.01$, the indentation effect is restricted to the region between $V / (E_s M)^{1/2} \approx 0.002$ and $V / (E_s M)^{1/2} \approx 0.004$. As the normalized width of loading platen is increased, the structural efficiency of the sandwiches decreases.

4 Finite element simulation

4.1 Finite element model

To validate the accuracy of analytical predictions, 3D finite element simulations for 3CSPs under out-of-plane 4-point bending are carried out using the commercial code ABAQUS v6.10. Note that, for 3CSPs, the failure mode of face bucking could be captured on the top face sheet under 4-point bending, but not under 3-point bending. The sandwich panel has a basic unit that is repetitive in the *x*-direction, as shown in Figure 1(b). As a result, to save computing time, periodic unit is used to model the structure. In the current study, four groups of periodic units (eight specimens) are simulated for four failure modes: A1 and A2 for face buckling; B1 and B2 for face yielding; C1 and C2 for core buckling; and D1 and D2 for core yielding. Their geometric
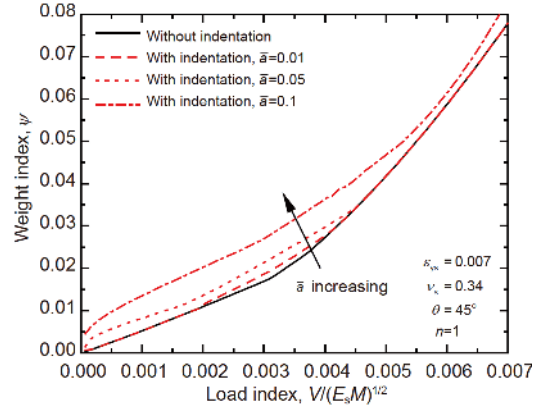
Figure 7 (Color online) Effect of loading platen width on optimal design on 3CSP subjected to generalized bending and indentation.

dimensions are listed in Table 1. As shown in Figure 8, the specimens are $L = 396$ mm in length, $B = 40$ mm in width, and $h = 20$ mm in height. The inclination angle θ is fixed at 45°, the aspect ratio $h / s = 1$, and the ratio $d / h = 1$. The lengths of loading span and support span are $L_p = 113$ mm and $L_b = 339$ mm, respectively.

With the corrugation webs assumed to be perfectly bonded with the face sheets, Boolean operation is used to merge the webs and face sheets together to create a single component. In the FE model (Figure 8), both the face sheets and the core webs are discretized using linear 3D reduced integration shell elements (S4R). Since the punches and bearings are much stiffer than the sandwiches, they are modeled as 3D analytical rigid shells. Ti-6Al-4V with $\varepsilon_{ys} = 0.007$ is selected as the base material and simulated using isotropic hardening elastoplasticity model with Young's modulus $E_s = 126$ GPa, yield stress $\sigma_{ys} = 889$ MPa, and Poisson ratio $v_s = 0.34$ [4]. The contacts between the top face sheet and the punches as well as those between the bottom face sheet and the bearings are defined as surface-to-surface contact interaction using the mechanical constraint formulation of kinematic contact method. Periodic boundary conditions are imposed at each end of the repeating unit in the *x*-direction. All the degrees of translational and rotational freedom on the edges $x = 0$ are equal to the corresponding ones on the edges $x = B$, as depicted schematically in Figure 8. Fixed boundary condition is applied to the reference point of each bearing. Mesh sensitivity study shows that an element size of 1.0 mm is sufficient for convergence. To investigate how the applied area of concentrated load affects the prediction accuracy, four different sizes of punch/bearing diameter are selected for simulation analysis. The results (details not shown here for brevity) demonstrate that the applied area of concentrated load has little influence on the prediction.

ABAQUS explicit solver is used to simulate the quasi-static bending of face sheet yielding and core web yielding.

Table 1 Geometric details of 3CSP specimens used in FE simulation

Specimen label	L^b (mm)	L^p (mm)	B (mm)	χ (mm)	t^f (mm)	t^c (mm)	h (mm)	d (mm)	s (mm)	θ (°)
A1	339	113	40	113	0.2	1	20	20	20	45
A2	339	113	40	113	0.4	1	20	20	20	45
B1	339	113	40	113	2	1	20	20	20	45
B2	339	113	40	113	2	0.8	20	20	20	45
C1	339	113	40	113	2	0.2	20	20	20	45
C2	339	113	40	113	2	0.3	20	20	20	45
D1	339	113	40	113	2	0.5	20	20	20	45
D2	339	113	40	113	2	0.4	20	20	20	45
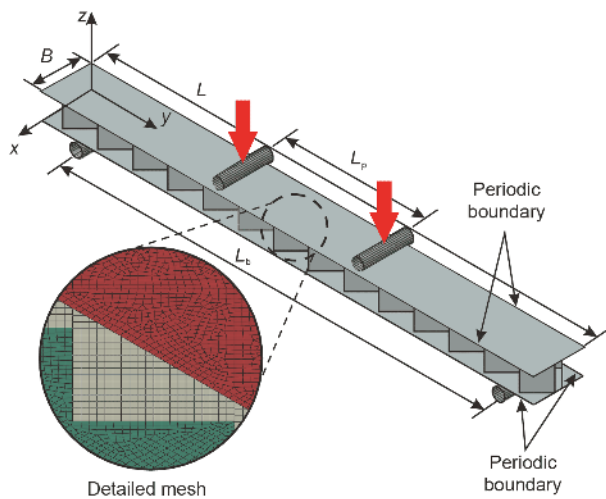
Figure 8 (Color online) Finite element model of 3CSP under longitudinal four-point bending.

Upon carrying out a loading rate independence study, the displacement rate of the punch is fixed at 0.1 m/s. To capture the elastic buckling of face sheet and core web, an eigenvalue analysis with the ABAQUS linear perturbation solver is also performed.

4.2 FE simulation results versus analytical model predictions

When subjected to longitudinal four-point bending (Figure 8), the typical collapse modes of the face sheets and the core webs are displayed in Figure 9. The elastic buckling modes of face sheet and core web are shown in Figure 9(a) and (c), respectively. As the segment between the two punches (Figure 9(a)) is a pure bending section, its top face sheet is subjected to uniform compression and the failure mode of face buckling occurs there. However, the segments between the punches and bearings are subjected to shear, and hence the shear buckling mode of flat plate occurs on the core web (Figure 9(c)).

Unlike buckling failure modes, the two failure modes of

face yielding (Figure 9(b)) and core yielding (Figure 9(d)) are hardly distinguishable from the deformation diagrams. For longitudinal four-point bending, Figure 10 presents the initial failure contours of face yielding and core yielding captured by FE calculations. The shear stress τ_{yz} of core web in specimen B1 is less than the shear yielding stress τ_{cy}. Nevertheless, the tensile stresses σ_y along the y-direction (shown in Figure 8) of the bottom face sheet in the pure bending section reaches the tensile yielding stress σ_{fy}. As a result, face yielding occurs, as shown in Figure 10(a). Similarly, core yielding occurs in specimen D1 as shown in Figure 10(b). For all the eight specimens considered, the failure modes and the corresponding initial failure loads are extracted from FE simulations, as listed in Table 2. In general, the failure modes and the initial failure loads obtained by FE calculations are in good agreement with the analytical model predictions.

5 Comparison of competing topologies

As a novel sandwich panel, it is instructive to compare the structural performance of the proposed 3CSPs under generalized bending with other competing lightweight sandwich constructions. As shown in Figure 11, five different core topologies are compared: corrugated channel core, corrugated core, hexagonal and square honeycombs, and lattice trusses. Results for 3CSPs loaded in longitudinally bending, corrugated sandwich panels loaded in longitudinal/transverse bending [10], and square honeycomb sandwich panels [30] have been restricted to a limited core thickness, $\bar{h} = 0.2$. Optimal design of the 3CSPs is performed using the geometry constraints of $d/h = 1$, $h/s = 1$ and $\theta = 45°$. Results for truss core panels and hexagonal honeycomb panels are taken from Wicks and Hutchinson [25]. All the results assume the base material is Ti-6Al-4V with $\varepsilon_{ys} = 0.007$. Analogous to the results presented in Sect. 3, the optimization results are all obtained using a SQP algorithm. For reference, the weight of an optimized solid plate is also
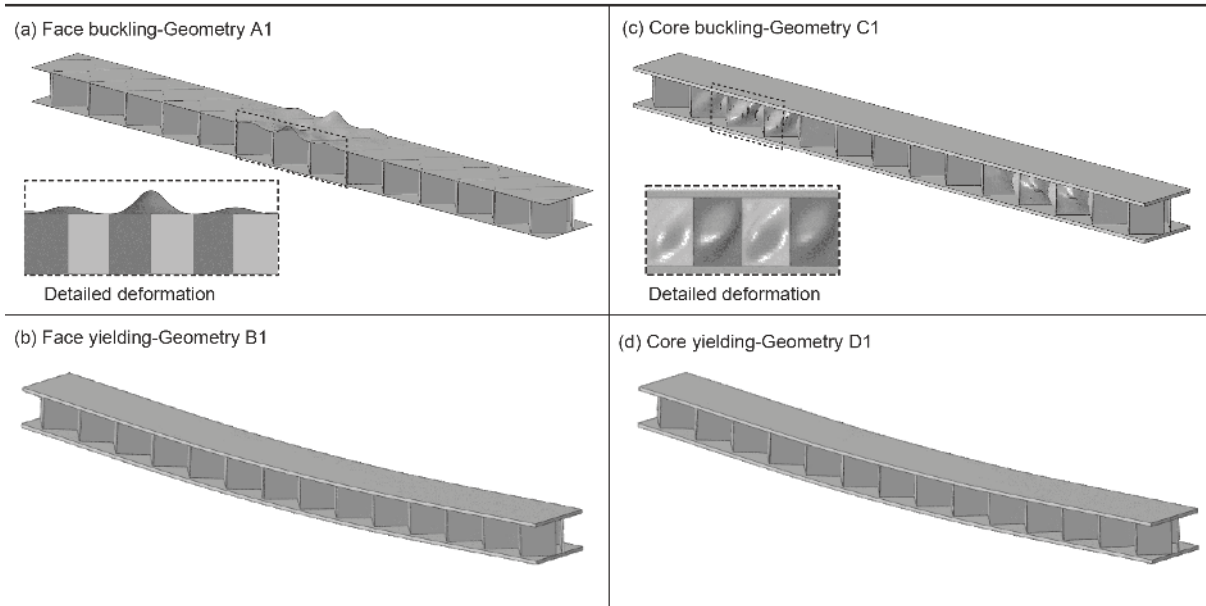
Figure 9 Typical failure modes of 3CSPs under longitudinal four-point bending captured by FE calculations: (a) face buckling for specimen A1; (b) face yielding for specimen B1; (c) core buckling for specimen C1; (d) core yielding for specimen D1.
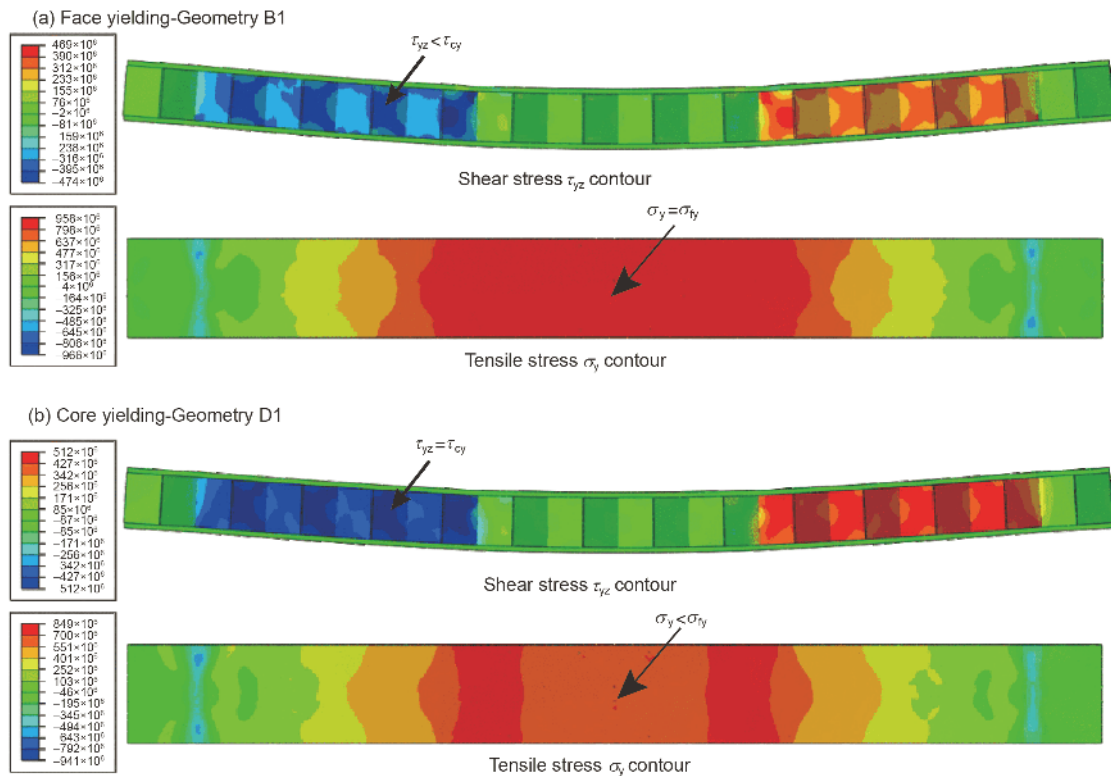
Figure 10 (Color online) Initial failure contours of face yielding and core yielding under longitudinal four-point bending captured by FE calculations: (a) face yielding for specimen B1; (b) core yielding for specimen D1.

included in Figure 11.

The results of Figure 11 reveal that the weight efficiency of 3CSPs is not only far superior to that of the solid plate, but also has significant advantage over the corrugated core, the truss core, and the square honeycomb, over the entire load range considered. In addition, although the hexagonal honeycomb exhibits the best performance at relatively low loads $(V/(E_sM)^{1/2} < 0.0015)$, the corrugated channel core per-

Table 2 Comparison between FE simulations and analytical predictions for 3CSPs under longitudinal four-point bending

Specimen label	Non-dimensional weight ψ	Failure mode		Non-dimensional load V^2/E_sM		
		Anal.	FE	Anal.	FE	Error
A1	0.0160	FB	FB	2.05×10^{-7}	2.15×10^{-7}	5%
A2	0.0196	FB	FB	1.65×10^{-6}	1.61×10^{-6}	−3%
B1	0.0479	FY	FY	2.43×10^{-5}	2.48×10^{-5}	2%
B2	0.0454	FY	FY	2.43×10^{-5}	2.46×10^{-5}	1%
C1	0.0379	CB	CB	2.42×10^{-6}	2.44×10^{-6}	1%
C2	0.0391	CB	CB	8.16×10^{-6}	8.16×10^{-6}	0%
D1	0.0416	CY	CY	1.80×10^{-5}	1.81×10^{-5}	1%
D2	0.0404	CY	CY	1.44×10^{-5}	1.49×10^{-5}	3%
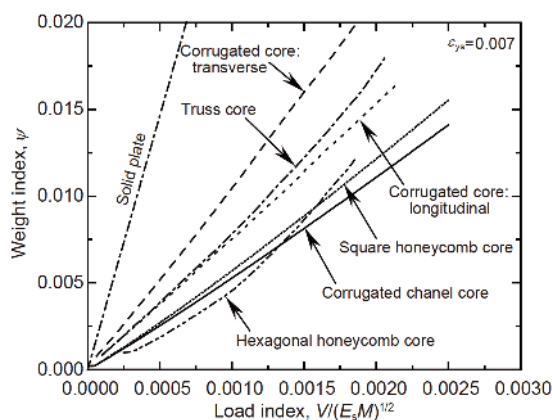
Figure 11 Comparison of minimum weight for different types of light-weight sandwich panel: 3CSP and corrugated panel loaded in longitudinal bending, corrugated panel loaded in transverse bending, hexagonal and square honeycomb panels, and truss core panels. The base material for all the panels is Ti-6Al-4V with $\varepsilon_{ys} = 0.007$.

forms better than all other topologies at higher loads, followed immediately by the square honeycomb. Therefore the proposed 3CSPs are strong competitors for load-bearing application demanding ultralightweight. When subjected to out-of-plane uniform compression, similar conclusion is reached as demonstrated in our previous study [4].

6 Conclusions

In the present study, we propose a new core topology, namely, the corrugated channel core, for ultralight multifunctional sandwich constructions. Optimization design based on strength failure mechanisms is carried out using a combined analytical and numerical approach for corrugated-channel-core sandwich panels (3CSPs) subject to generalized bending as well as indentation. The analytically predicted initial failure strengths and failure modes agree well with those obtained with direct finite element simulations. The influence of key geometrical and material properties is systematically studied. It is demonstrated that the corrugated

channel core exhibits superior structural efficiency relative to such common sandwich core topologies as corrugations, hexagonal and square honeycombs, and lattice trusses. From the heat transfer point of view, the corrugated channels are also superior to conventional parallel plate channels (commonly applied for active cooling) under the design criteria of equal mass flow rate, equal pressure drop, and equal pumping power. Therefore, the proposed 3CSPs hold great potential for multifunctional applications, e.g., simultaneous load bearing and active cooling.

The present assessment for 3CSPs has the limitation that only longitudinal loading is considered. In many practical situations, transverse loading should also be considered. In the transverse direction, the core webs are discontinuous, the assumptions listed in Sect. 2.1 do not hold, and the frame analysis should be used. In addition to carrying structural loads, the 3CSP can also effectively dissipate heat as demonstrated in ref. [22]. The results can be combined to obtain minimum weight designs subject to the constraint of simultaneous structural loading and heat dissipation. These issues will be addressed in a follow-up research.

Appendix: Indentation model

For the indentation failure mode, local loading is transmitted to the corrugated channel core through deformation of the face sheet by a loading platen with width a. In general, indentation failure is accompanied by the formation of plastic hinges and compressive collapse of the underlying core [31]. Correspondingly, the collapse load of indentation is

$$V = 2t_{\mathrm{f}}\sqrt{\sigma_{\mathrm{ys}}\Sigma_{\mathrm{I}}} + a\Sigma_{\mathrm{I}}, \tag{a1}$$

where Σ_{I} is the compressive strength of the core, given by [4]

$$\Sigma_{\mathrm{I}} = \begin{cases} \dfrac{6.74\pi^2 E_{\mathrm{s}}}{12\left(1-v_{\mathrm{s}}^2\right)}\left(\dfrac{t_{\mathrm{c}}}{s}\right)^2 \overline{\rho}, & \text{core buckling,} \\[4mm] \sigma_{\mathrm{ys}}\overline{\rho}, & \text{core yielding,} \end{cases} \tag{a2}$$

where $\overline{\rho} = \dfrac{t_{\mathrm{c}}}{d\cos\theta}$. The non-dimensional form of eq. (a1) is

$$\frac{V^2}{E_{\mathrm{s}}M} = 2\overline{t}_{\mathrm{f}}\sqrt{\frac{\sigma_{\mathrm{ys}}}{E_{\mathrm{s}}}\frac{\Sigma_{\mathrm{I}}}{E_{\mathrm{s}}}} + \overline{a}\frac{\Sigma_{\mathrm{I}}}{E_{\mathrm{s}}}, \tag{a3}$$

where $\overline{a} = a/\chi$ is the normalized width of loading platen. Upon substituting $h/s = 1$, $d/h = n$ and eq. (a2) into eq. (a3), the non-dimensional form of indentation failure criteria become

$$\frac{V^2}{E_{\mathrm{s}}M} = \begin{cases} 2\overline{t}_{\mathrm{f}}\sqrt{\varepsilon_{\mathrm{ys}}\dfrac{6.74\pi^2}{12\left(1-v_{\mathrm{s}}^2\right)}\left(\dfrac{\overline{t}_{\mathrm{c}}}{\overline{h}}\right)^3\dfrac{1}{n\cos\theta}} \\[4mm] +\overline{a}\dfrac{6.74\pi^2}{12\left(1-v_{\mathrm{s}}^2\right)}\left(\dfrac{\overline{t}_{\mathrm{c}}}{\overline{h}}\right)^3\dfrac{1}{n\cos\theta}, \\[2mm] \qquad\qquad \text{core buckling,} \\[3mm] 2\overline{t}_{\mathrm{f}}\sqrt{\varepsilon_{\mathrm{ys}}\varepsilon_{\mathrm{ys}}\dfrac{\overline{t}_{\mathrm{c}}}{\overline{h}}\dfrac{1}{n\cos\theta}} + \overline{a}\varepsilon_{\mathrm{ys}}\dfrac{\overline{t}_{\mathrm{c}}}{\overline{h}}\dfrac{1}{n\cos\theta}, \\[2mm] \qquad\qquad \text{core yielding.} \end{cases} \tag{a4}$$

Upon adding eq. (a4) into eq. (9), the minimum weight design of 3CSP subject to simultaneous generalized bending and indentation is performed using the SQP algorithm coded in MATLAB.

1   Lu T, Valdevit L, Evans A. Active cooling by metallic sandwich structures with periodic cores. Prog Mater Sci, 2005, 50: 789–815

2   Han B, Zhang Z J, Zhang Q C, et al. Recent advances in hybrid lattice-cored sandwiches for enhanced multifunctional performance. Extreme Mech Lett, 2017, 10: 58–69

3   Zhang Q, Yang X, Li P, et al. Bioinspired engineering of honeycomb structure—Using nature to inspire human innovation. Prog Mater Sci, 2015, 74: 332–400

4   Zhao Z, Han B, Wang X, et al. Out-of-plane compression of Ti-6Al-4V sandwich panels with corrugated channel cores. Mater Des, 2018, 137: 463–472

5   Kim T, Zhao C Y, Lu T J, et al. Convective heat dissipation with lattice-frame materials. Mech Mater, 2004, 36: 767–780

6   Kim T, Hodson H P, Lu T J. Fluid-flow and endwall heat-transfer characteristics of an ultralight lattice-frame material. Int J Heat Mass Transfer, 2004, 47: 1129–1140

7   Yan H B, Zhang Q C, Lu T J. An X-type lattice cored ventilated brake disc with enhanced cooling performance. Int J Heat Mass Transfer, 2015, 80: 458–468

8   Yan H B, Zhang Q C, Lu T J. Heat transfer enhancement by X-type lattice in ventilated brake disc. Int J Thermal Sci, 2016, 107: 39–55

9   Guo R, Zhang Q C, Zhou H, et al. Progress in manufacturing light-weight corrugated sandwich structures and their multifunctional applications. Mech Eng, 2017, 39: 226–239

10 Valdevit L, Hutchinson J W, Evans A G. Structurally optimized sandwich panels with prismatic cores. Int J Solids Struct, 2004, 41: 5105–5124

11 Valdevit L, Wei Z, Mercer C, et al. Structural performance of near-optimal sandwich panels with corrugated cores. Int J Solids Struct, 2006, 43: 4888–4905

12 Côté F, Deshpande V S, Fleck N A, et al. The compressive and shear responses of corrugated and diamond lattice materials. Int J Solids Struct, 2006, 43: 6220–6242

13 Tian Y S, Lu T J. Optimal design of compression corrugated panels. Thin-Walled Struct, 2005, 43: 477–498

14 Lu T J. Heat transfer efficiency of metal honeycombs. Int J Heat Mass Transfer, 1999, 42: 2031–2040

15 Gu S, Lu T J, Evans A G. On the design of two-dimensional cellular metals for combined heat dissipation and structural load capacity. Int J Heat Mass Transfer, 2001, 44: 2163–2175

16 Valdevit L, Pantano A, Stone H A, et al. Optimal active cooling performance of metallic sandwich panels with prismatic cores. Int J Heat Mass Transfer, 2006, 49: 3819–3830

17 Wen T, Xu F, Lu T J. Structural optimization of two-dimensional cellular metals cooled by forced convection. Int J Heat Mass Transfer, 2007, 50: 2590–2604

18 Liu T, Deng Z C, Lu T J. Minimum weights of pressurized hollow sandwich cylinders with ultralight cellular cores. Int J Solids Struct, 2007, 44: 3231–3266

19 Liu T, Deng Z C, Lu T J. Bi-functional optimization of actively cooled, pressurized hollow sandwich cylinders with prismatic cores. J Mech Phys Solids, 2007, 55: 2565–2602

20 Tan X H, Soh A K. Multi-objective optimization of the sandwich panels with prismatic cores using genetic algorithms. Int J Solids Struct, 2007, 44: 5466–5480

21 Rathbun H J, Zok F W, Evans A G. Strength optimization of metallic sandwich panels subject to bending. Int J Solids Struct, 2005, 42: 6643–6661

22 Ali M M, Ramadhyani S. Experiments on convective heat transfer in corrugated channels. Exp Heat Transfer, 1992, 5: 175–193

23 Hassanein M F, Kharoob O F. Shear buckling behavior of tapered bridge girders with steel corrugated webs. Eng Struct, 2014, 74: 157–169

24 Driver R G, Abbas H H, Sause R. Shear behavior of corrugated web bridge girders. J Struct Eng, 2006, 132: 195–203

25 Wicks N, Hutchinson J W. Optimal truss plates. Int J Solids Struct, 2001, 38: 5165–5183

26 Chen J. Stability Theory and Design of Steel Structure. Beijing: Science Press, 2014

27 Timoshenko S P, Gere J M, Prager W. Theory of Elastic Stability. 2nd ed. New York: McGraw-Hill Book Co, 1961

28 Han B, Qin K K, Yu B, et al. Design optimization of foam-reinforced corrugated sandwich beams. Composite Struct, 2015, 130: 51–62

29 Zok F W, Rathbun H J, Wei Z, et al. Design of metallic textile core sandwich panels. Int J Solids Struct, 2003, 40: 5707–5722

30 Zok F W, Rathbun H, He M, et al. Structural performance of metallic sandwich panels with square honeycomb cores. Philos Mag, 2005, 85: 3207–3234

31 Ashby M F, Evans A, Fleck N A, et al. Metal Foams: A Design Guide. Oxford: Butterworth-Heinemann, 2000